Mitigation of Two-Plasmon Decay in Direct-Drive Inertial Confinement Fusion Through the Manipulation of Ion-Acoustic- and Langmuir-Wave Damping

Introduction

Two-plasmon decay[1–6] (TPD) is a three-wave–decay instability in which an electromagnetic (EM) wave parametrically decays into two longitudinal (Langmuir) waves. Experimentally, signatures of TPD have been observed in the ionosphere[7] and in laser–plasma interaction experiments.[8,9] In the context of laser fusion, TPD has been identified in both the indirect-[10] and direct-drive[11] approaches.In these schemes, TPD is undesirable because of the anomalous absorption of laser light at densities below the critical density and the potential to accelerate electrons to high energies.[12–16] High-energy electrons can preheat the target and severely degrade performance since efficient implosions require the fuel to remain on a low adiabat.

The linear stability of a single-plane EM wave subject to TPD has been studied for quite some time,[1–6,17,18] although not without controversy regarding its absolute/convective nature in inhomogeneous plasma.[16,19,20] In TPD, a photon decays into two plasmons, fulfilling the frequency- and wave-number–matching conditions, $\omega_0 = \omega + \omega'$, $\vec{k}_0 = \vec{k} + \vec{k}'$, where ω_0 and $\vec{k}_0 \left(k_0 \equiv \left| \vec{k}_0 \right| = \omega_0 \big/ c\sqrt{1 - n_e \big/ n_c} \right)$ are the frequency and wave vector, respectively, of an EM wave in a plasma having an electron number density n_e relative to the critical density $n_c \left[= m_e \omega_0^2 \big/ (4\pi e^2) \right]$ at which EM waves are evanescent. Here, e and m_e are the electron charge and mass, respectively, and c is the speed of light. The quantities ω, ω', $\vec{k}$, and $\vec{k}'$ are the frequencies and wave vectors of the two decay Langmuir waves (LW's) (note that in the literature, the terms "Langmuir wave," "plasma wave," and "plasmon" are used interchangeably). The essential features are described by the temporal TPD growth rate γ (in the presence of LW damping rate ν_e):

$$\gamma = \gamma_0 - \nu_e = \frac{\vec{k} \cdot \vec{v}_{osc}}{4} \frac{\left[\left(\vec{k}_0 - \vec{k} \right)^2 - k^2 \right]}{k \left| \vec{k}_0 - \vec{k} \right|} - \nu_e , \qquad (1)$$

where $\vec{v}_{osc} = e\vec{E}_0 \big/ \omega_0 m_e$ is the oscillation velocity of an electron in the electric field of the plane EM wave $\vec{E}_0$. The relation between $k_\parallel$ and $k_\perp$ (parallel and perpendicular components of $\vec{k}$ with respect to $\vec{k}_0$) corresponding to maximum growth defines a hyperbola in k space, $\vec{k}_\perp^{\,2} = k_\parallel (k_\parallel - k_0)$. From Eq. (1) it can be seen that two-plasmon decay cannot be studied in one spatial dimension (since $\vec{k}_0 \cdot \vec{v}_{osc} = 0$ for EM waves). For this reason most, if not all, numerical calculations to date have been performed in 2-D in the plane of maximum growth, i.e., the plane of polarization (such is the case here).

In experiments utilizing multiple overlapping laser beams, the instability is believed to be driven cooperatively by several beams[21] through the sharing of common TPD waves.[22–24] To retain this feature in two spatial dimensions, all calculations were performed with two EM waves arranged symmetrically about the density gradient with angles of ±23° (as in previous work[25–28]).

Parametric instabilities occur when the pump amplitude exceeds a threshold that depends on collisional effects, Landau damping, and plasma inhomogeneity. The effect of collisional damping of LW's was not emphasized in earlier theoretical works. This was either for simplicity or motivated by the dominance of inhomogeneity in experiments. In this work, all three effects are included.

In several previous studies of the nonlinear saturation of electromagnetically driven parametric instabilities, the level of LW excitation was seen to depend on the ion-acoustic–wave (IAW) damping rate. This was reported in detail in simulations of the nonlinear stage of stimulated Raman scattering (SRS) in laser hot spots,[29] in regimes of low Landau damping of the Langmuir wave. It was found that the SRS reflectivity increased linearly with the IAW damping rate. In general, the development of Langmuir turbulence and collapse physics is known to depend on the ion-acoustic damping rate.[30–32] These earlier results suggest that TPD could be less severe in materials with high collisional damping of LW and weak collisional damping of IAW (experimental evidence suggests TPD suppression in mid-Z targets[33,34]). More importantly, there could be practical implications for directly driven inertial confinement fusion (ICF) since Betti[35] and Lafon[36] have shown that igniting targets

can be designed using mid-Z ablators at the megajoule (MJ) scale. These could provide an alternate path to ignition should TPD preheat be too high in directly driven designs using plastic (CH) ablators.[37]

The following sections describe the numerical "*QZAK*" model and explain in detail the approximations that have been made; the properties of linear stability; and the anomalous absorption of hot-electron production that is characteristic of the nonlinearly saturated state, emphasizing the sensitivity to plasma conditions, followed by a summary and discussion.

Numerical Simulation of TPD Growth and Saturation in Inhomogeneous Collisional Plasma

Zakharov models[38,39] have been used extensively to study the evolution of Langmuir waves and their nonlinear coupling with ion-acoustic waves, particularly LW self-focusing and collapse. The Zakharov model describes both three- and four-wave interactions,[40] which have been used to study strong Langmuir turbulence[41,42] relevant to laboratory plasmas,[43,44] ionospheric modification experiments,[30,31,45] laser-plasma experiments,[32,46,47] and pulsar radio emissions.[48] The weak turbulence regime[40] assumes random phase interactions between the linear modes and does not accurately describe the results from Zakharov models[49] because of strong turbulence effects. The strong turbulence regime[41,42] involves phase-coherent interactions including self-focusing, cavitation, and collapse, which can coexist[50] with wave–wave processes such as the Langmuir decay instability (LDI).[40,51] The key approximation of the model is that of temporal enveloping. The fast variations ($\partial/\partial t \sim \omega_{pe}$) of the LW electrostatic field are explicitly removed, and the slow variations ($\partial/\partial t \ll \omega_{pe}$) are followed by the complex-valued function, or "envelope" $\vec{E}_1(\vec{x},t)$. For example, the physical LW electrostatic field $\vec{E}$ is given by $\vec{E} = 1/2\left[\vec{E}_1(\vec{x},t)\exp\left(-i\omega_{pe}t\right) + \text{c.c.}\right]$, which is centered at the reference plasma frequency $\omega_{pe} = (4\pi n_0 e^2/m_e)^{1/2}$.

In the extended quasi-linear Zakharov model of TPD,[32,46] multiple envelopes are defined by an expansion in harmonics of the reference electron plasma frequency ω_{pe} (which is itself defined in terms of a reference density n_0). This is useful since TPD is localized between a narrow range of densities in the neighborhood of $n_c/4$. Two envelopes and a low-frequency term are sufficient for the present analysis,[52] shown below for the plasma current:

$$\vec{J}(\vec{x},t) = \vec{J}_0(\vec{x},t) + \frac{1}{2}\left[\vec{J}_1(\vec{x},t)\exp\left(-i\omega_{pe}t\right) + \vec{J}_2(\vec{x},t)\exp\left(-i2\omega_{pe}t\right) + \text{c.c.}\right], \quad (2)$$

where $\left|\partial\vec{J}_1/\partial t\right| \ll \omega_{pe}\left|\vec{J}_1\right|$, etc. The term proportional to $\vec{J}_1$ is centered at the plasma frequency ω_{pe} and therefore close to one half of the laser frequency. The longitudinal component of $\vec{J}_1$ drives the first Zakharov equation (LW response), while the transverse component is responsible for the $\omega_0/2$ radiation[53–56] (including SRS[29] and the mixed-polarization, high-frequency hybrid instability[18]). The term $\vec{J}_2$, near twice the plasma frequency $2\omega_p$ and therefore close to the laser frequency ω_0 (with mismatch $\Delta\omega \equiv \omega_0 - 2\omega_{pe} \ll 2\omega_p$), modifies the laser propagation and is the source of pump depletion. [The subscript "0" denoting the laser frequency ω_0 throughout is not to be confused with the subscript "0" in Eq. (2), where it denotes terms with a frequency far below the electron plasma frequency.] The plasma response to low-frequency terms is assumed to be quasi-neutral $\delta n = \delta n_e \approx Z\delta n_i$, where Z is the ion charge and δn_e and δn_i are the electron- and ion-density perturbations, respectively. Inhomogeneous plasmas with a weak density gradient are investigated by the addition of a static term describing density perturbations from the reference density (as described in Russell *et al.*[46]) and by a constant flow velocity $\vec{u}_0$.

The primary disadvantage of a fluid-moment model such as the Zakharov model[32,46] is the lack of nonlinear kinetic saturation mechanisms. Although often derived from the plasma fluid equations,[57] *ZAK*[25,26,32,46] and also the *QZAK* (described below) and RPIC numerical codes (described in Vu *et al.*[25]) can be shown to be direct consequences of the Vlasov equation by the use of a multiple time-scale analysis and the requirement that certain parameters remain "small," e.g., $|\vec{E}_1|^2/(4\pi n_0 T_e) < 1$, $\delta n_0/n_{e0} < 1$, and $k\lambda_{De} < 1$ (Ref. 58), where

$$\lambda_{De} = \sqrt{T_e/(4\pi n_0 e^2)}$$

is the electron Debye length. The *ZAK* model of TPD[25,26,32,46] [which includes linear wave–particle interactions (Landau damping)] is improved upon by *QZAK*, which evolves the electron-distribution function in the quasi-linear approximation. RPIC is a time-enveloped particle-in-cell (PIC) code that improves on *QZAK* since it does not make the quasi-linear approximation.[25] When the proper conditions are met, the predictions of RPIC and *QZAK* should agree. Since PIC codes generally make no small-parameter assumptions, they can be used to check the validity of *QZAK* calculations. This was discussed in a recent paper by Vu *et al.*[27] using the code RPIC and also briefly in **Confirmation of the Sensitivity to**

Ion-Acoustic Damping Using RPIC Calculations (p. 122) (unlike typical PIC codes, RPIC assumes that a separation of time scales exists, which could in some sense be considered as an expansion parameter).

The Extended Quasi-Linear Zakharov (QZAK) Model of TPD

The harmonic decomposition in ω_{pe} suggested by Eq. (2) leads to the following equation for EM waves having frequencies of $2\omega_{pe}$ (i.e., near that of the laser pump):

$$\left\{-2i\left(2\omega_p\right)\left(\partial_t+\nu_{2,T}\right)+c^2\nabla^2+\left(2\omega_{pe}\right)^2 \times\left[1-\left(n_0+\delta N+\delta n\right)\Big/\left(4n_0\right)\right]\right\}\vec{E}_{2,T} =\left(e\big/m_e\right)\left[\left(\nabla\bullet\vec{E}_1\right)\vec{E}_1\right]_T. \quad (3)$$

This equation describes the laser pump field, which is imposed as a boundary condition, together with other components resulting from nonlinearities. The relation of the laser electric field $\vec{E}_0$ to the transverse component of the second-harmonic envelope is given by $\vec{E}_0=\vec{E}_{2,T}\exp\left(i\Delta\omega t\right)$, where $\Delta\omega$ represents the slight frequency mismatch that arises because n_0 (= 0.23 n_c) is slightly less than $n_c\big/4$ (to allow for the density gradient). The subscript "T" denotes the transverse component, which is most easily expressed in Fourier space: $\vec{E}_{2,T}\left(\vec{k}\right)=\left(\vec{I}-\vec{k}\vec{k}\big/k^2\right)\bullet\vec{E}_2\left(\vec{k}\right)$. The quantity $\nu_{2,T}$ is the collisional damping rate of transverse waves $\nu_{2,T}\approx\left(n_0\big/n_c\right)\nu_{ei}$ that gives rise to inverse-bremsstrahlung absorption,[59] where

$$\nu_{ei}\approx 3\times10^{-6}\log\left(\lambda\right)\left(n_e\big/1\,\mathrm{cm}^{-3}\right)Z\Big/\left(T_e\big/1\,\mathrm{eV}\right)^{3/2}$$

is the usual electron–ion collision frequency (in s^{-1}), where $\log(\lambda)$ is the Coulomb logarithm and T_e is the electron temperature. The term $\delta N\left(\vec{x}\right)$ is a small, nonevolving density perturbation describing the weakly inhomogeneous density,[46] while $\delta n\left(\vec{x},t\right)$ is the quasi-neutral piece that is driven by the ponderomotive pressure of the high-frequency fluctuations. The total low-frequency density is given by $n_e\left(\vec{x},t\right)=n_0+\delta N\left(\vec{x}\right)+\delta n\left(\vec{x},t\right)$ with the assumption that both $\delta N/n_0\ll1$ and $\delta n/n_0\ll1$. In all calculations presented here, δN varies linearly in the x direction only (the "longitudinal" direction), while the initial density scale length $L_n\equiv\left[\mathrm{d}/\mathrm{d}x\,\ln(n_0+\delta N)\right]^{-1}=330\,\mu$m (at box center) unless otherwise noted. The right-hand side of Eq. (3) describes the depletion of $\vec{E}_{2,T}$ as a result of its decay into electrostatic waves $\vec{E}_1$.

In two-plasmon decay it is likely that the background particle-distribution functions are significantly changed during the nonlinear stage of the instability. High levels of LW's or IAW's can lead to important modifications of the electron and ion distribution functions; these modifications, in turn, affect the nonlinear levels of the wave excitation. A multiple time-scale analysis of the spatially averaged electron Vlasov equation, together with a quasi-neutral low-frequency response, leads to the same coupled envelope equations for the electrostatic response:

$$\nabla\bullet\left[2i\omega_{pe}\left(D_t+\nu_e\circ\right)+3v_e^2\nabla^2-\omega_{pe}^2\left(\delta n+\delta N\right)\big/n_0\right]\vec{E}_1 =\left(\frac{e}{4m_e}\right)\nabla\bullet\left[\nabla\left(\vec{E}_0\bullet\vec{E}_1^*\right)-\vec{E}_0\nabla\bullet\vec{E}_1^*\right]e^{-i\Delta\omega t}+S_E, \quad (4)$$

(described by $\vec{E}_1$) and for the low-frequency response

$$\left[D_t^2+2\nu_i\circ D_t-c_s^2\nabla^2\right]\delta n=\frac{Z}{16\pi m_i}\nabla^2\left(\left|\vec{E}_1\right|^2+\frac{1}{4}\left|\vec{E}_0\right|^2\right), \quad (5)$$

as described previously[32] [with the exception of the terms representing inhomogeneity (discussed in more detail below)]. The important difference is that the linear response [i.e., the coefficients on the left-hand side of Eqs. (4) and (5)] varies over times that are long compared with the variation of the envelopes. In both Eqs. (4) and (5), $D_t\equiv\left(\partial_t+\vec{u}_0\bullet\nabla\right)$ is the convective derivative and the term S_E is the time-random-phase Čerenkov noise source[60] for Langmuir waves as described in Russell *et al.*[46] Noise enters the acoustic-wave equation only through the LW ponderomotive force. In Eq. (4), $\nu_e=\nu_{coll}+\gamma_L$ is the sum of the collisional and Landau damping for LW's (which evolves in time) and whose dispersion depends on the electron thermal velocity $v_e=\sqrt{T_e\big/m_e}$. The first term on the right-hand side is the longitudinal part of the nonlinear current $\vec{J}_1$, which drives density perturbations with frequencies close to ω_{pe}. In Eq. (5), $c_s=\left(ZT_e\big/m_i\right)^{1/2}\left(1+\gamma_iT_i\big/ZT_e\right)$ is the speed of ion-acoustic waves that damp with the rate ν_i, where $\gamma_i\approx3$, m_i, and T_i are the ion ratio of specific heats, mass, and temperature, respectively. The first term on the right-hand side describes the low-frequency ponderomotive forces of Langmuir and electromagnetic fluctuations.

As in the work of Sanbonmatsu *et al.*,[61] the slow temporal evolution of the spatially averaged electron distribution func-

tion $\langle F_e \rangle$, which is a function of velocity $\vec{v}$ and time t only, is governed by a Fokker–Planck equation:

$$\partial_t \langle F_e \rangle + \nu(\vec{v})\left(\langle F_e \rangle - F_0\right) = \partial_{\vec{v}} \cdot \left[\hat{D}(\vec{v}) \cdot \partial_{\vec{v}} \langle F_e \rangle\right] + \partial_{\vec{v}} \cdot (\delta\hat{D} \cdot \vec{v}) \langle F_e \rangle / v_e^2 + \hat{\sigma}_{IB}\left[\left|\vec{E}_1\right|^2\right] + \hat{\sigma}_{IB}\left[\left|\vec{E}_2\right|^2\right]. \quad (6)$$

The diffusion coefficient $\hat{D}(\vec{v})$ is given by the usual quasi-linear form:

$$\hat{D}(\vec{v}) \approx D_{QL}(\vec{v}) = \frac{\pi e^2 |\Delta\vec{k}|}{2m_e^2 \Delta k_x \Delta k_y} \sum_{k:\left(\omega_{pe} - \vec{k}\cdot\vec{v} = 0\right)} \frac{\vec{k}\vec{k}}{|\vec{v}|} \left|\psi_1(\vec{k})\right|^2, \quad (7)$$

where $\psi_1(\vec{k})$ is the electrostatic potential $\vec{E}_1(\vec{k},t) = -i\vec{k}\psi_1(\vec{k},t)$. The quantity $\Delta\vec{k}$ is the wave-vector spacing along the line in k space defined (for given $\vec{v}$) by the constraint $\omega_{pe} - \vec{k}\cdot\vec{v} = 0$, while Δk_x and Δk_y are equal to $2\pi/L_x$ and $2\pi/L_y$, respectively. The quantities L_x and L_y are the lengths of the simulation domain in the x and y directions. The second term on the left-hand side of Eq. (6) involving the term $\nu(\vec{v}) \equiv s_x |v_x| / L_x + s_y |v_y| / L_y$, with s_x, s_y taking the values of either 0 or 1, is the result of spatially averaging the advective term in the kinetic equation for the distribution function over the domain in which Eqs. (4) and (5) are solved: $[0, L_x] \times [0, L_y]$ (Ref. 61). If the calculation is periodic in the y direction, for example, the corresponding contribution to this term vanishes (i.e., $s_y = 0$). It is assumed that the outgoing distribution of velocities at each spatial boundary is the same as the spatially averaged distribution function.[27] The term $\delta\hat{D}$ entering into Eq. (6) has the same definition as $\hat{D}$ in Eq. (7), but it is calculated with the initial LW noise spectrum to ensure that $\langle F_0 \rangle$ is a steady-state solution to the undriven Eqs. (4)–(7) as described in Sanbonmatsu *et al.*[61] *Ad hoc* differential operators $\hat{\sigma}_{IB}\left[\left|\vec{E}_1\right|^2\right]$, $\hat{\sigma}_{IB}\left[\left|\vec{E}_2\right|^2\right]$, which have been added to Eq. (6), are intended to correspond to the collisional absorption of LW and EM waves, described by the envelopes $\vec{E}_1$ and $\vec{E}_2$, respectively, since they can become important for collisional plasmas. The form of these operators is left unspecified.

The distribution function $\langle F_e \rangle(\vec{v},t)$, which evolves according to Eq. (6) starting from the initial condition $\langle F_e \rangle(\vec{v},t) = F_0$, redefines the linear response of the plasma in time through the linear susceptibilities that modify the frequencies (e.g., c_s and v_e) and damping rates (γ_L) of the linear modes. In the current implementation of *QZAK*, only the electron Landau damping [entering into ν_e of Eq. (4)] is evolved:

$$\gamma_L(\vec{k},t) \approx \frac{\pi\omega_{pe}^2}{k^2} \int d\vec{v}\vec{k} \cdot \partial_{\vec{v}} \langle F_e \rangle(\vec{v},t) \delta\left(\omega_{pe} - \vec{k}\cdot\vec{v}\right). \quad (8)$$

Equations (3)–(8) are solved in two spatial dimensions by a split-step method. Equation (3) is currently solved by neglecting collisional absorption, pump depletion, and nonlinear terms (i.e., trivially), while Eqs. (4) and (5) are advanced by a pseudospectral method:[62,63] All the linear propagation terms of Eqs. (4) and (5) are computed in Fourier space (Landau damping can be easily written in k space), while the nonlinear term in Eq. (4) is updated in real space. Both the transverse (y direction) and longitudinal (x direction) boundary conditions for the fields $\vec{E}_1$ and δn are assumed to be periodic. Physically, the longitudinal direction should be open. In the longitudinal direction the LW's are strongly damped, however, in the low-density region due to Landau damping, and they are evanescent beyond the quarter-critical density, so there is actually negligible cross-communication and differences between periodic and outgoing boundary conditions should be negligible. Ion fluctuations are strongly damped at both longitudinal boundaries by the addition of a "beach" to ensure there is no recirculation.[29] This can be important for weakly damped IAW.

The distribution function $\langle F_e \rangle$ is updated less frequently than the envelopes by evolving Eq. (6), neglecting the inverse bremsstrahlung operators, using an alternating-direction implicit (ADI) scheme.[64] At each update of Eq. (6), the Landau-damping term γ_L is updated according to Eq. (8). Although Eqs. (6)–(8) have been written here in the nonrelativistic approximation (for clarity), *QZAK* actually solves their relativistic generalization.

A major assumption used in the derivation of Eq. (6) was that the electron-distribution function is well approximated by its spatial average. It is not evident that this should be so, given that the plasma is (weakly) inhomogeneous. However, recent results using the time-enveloped particle-in-cell code RPIC indicate this to be a valid assumption.[27] This important simplification is very beneficial because it makes large-scale simulations of the nonlinear evolution of TPD using Eqs. (3)–(8) practical, particularly in three dimensions. Three-dimensional simulations are important

since it has been demonstrated that the TPD process is driven by the mutual interaction of multiple laser beams.[21,23,24]

The self-consistent set of equations [Eqs. (3)–(8)] reach, in many cases, a statistical steady state in which it is possible to associate a heat flux associated with suprathermal particles and an anomalous absorption because of all the dissipative processes. Solutions to the velocity-space diffusion equation [Eqs. (6) and (7)] allow one to estimate hot-electron production, which is important if connections are to be made with experiment[16,24,65] and other kinetic modeling.[25,27,28,66–68]

Aspects of Linear Stability

Two-plasmon decay in a strictly linearly varying density profile was first found to be convectively unstable using an analysis based on the spatial envelope approximation.[2] Later, Simon *et al*.,[6] arguing that the spatial envelope approximation becomes invalid near the LW turning point, showed that two-plasmon decay of a plane EM wave propagating in the direction of the density gradient is absolutely unstable.[3,6,17,69,70] The correct threshold intensity was obtained by Simon *et al*.[6] and is given approximately by

$$I_{14} \approx 1.4\left(T_e \big/ 2\ \text{keV}\right) \big/ \left(L_n \big/ 330\ \mu\text{m}\right) \qquad (9)$$

for conditions of current experiments,[16] where I_{14} is the laser intensity in units of 10^{14} W/cm^2 and L_n is the density scale length. This threshold condition is plotted in Fig. 134.35. The TPD instability extends to wave numbers outside the region of absolute instability to include modes that have been determined to be convectively unstable,[24,67] with the convective "threshold" intensity a factor of a few times higher for a single-plane EM wave pump.[67] These works[6,24,67] neglected the damping of the decay plasma waves. As can be seen in Fig. 134.35, this is a good approximation since the damping threshold intensity is much smaller than the inhomogeneity threshold at the scale accessible by ~10- to 20-kJ lasers (e.g., OMEGA[71]/OMEGA EP[72]) indicated by the yellow shaded region.

In the opposite (homogeneous) limit, the damping threshold (also shown in Fig. 134.35) is simply given by $\gamma_0 \gtrsim \nu_{ei}/2$ (cf., e.g., Goldman[1,73] or Kruer[74]) since collisional damping $\nu_{coll} \sim \nu_{ei}/2$ greatly exceeds Landau damping γ_L for wave numbers $k \lesssim 0.25\, k_D$ in a Maxwellian plasma $\left(\text{i.e.}, \nu_e \approx \nu_{ei}/2\right)$, where γ_0 is the temporal growth rate and $k_D = 1/\lambda_{De}$ is the Debye wave number. A stability analysis of Eq. (4) performed for a single-plane EM wave and taking $\delta N = 0$ can be shown to give

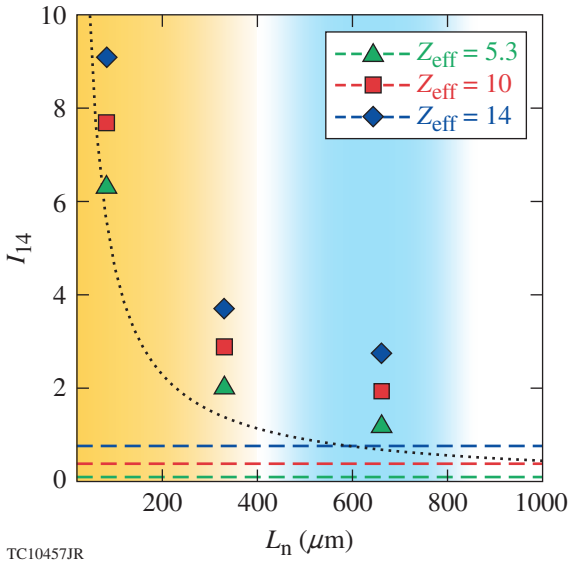

Figure 134.35
The markers show the numerically determined threshold for absolute two-plasmon–decay (TPD) instability of two plane electromagnetic (EM) waves incident at angles of ±23° with respect to a density gradient of scale length L_n for different values of Z_{eff} [and, therefore, collisional Langmuir-wave (LW) damping]. The plotted intensity is the sum of the single-beam intensities. For comparison, the dotted line shows the approximate absolute threshold intensity, in the absence of LW damping, for a single, normally incident plane EM wave[6] as a function of density scale length. The collisional threshold in the absence of plasma inhomogeneity is shown by the horizontal dashed lines for various Z_{eff}. In all cases, the electron temperature is given by $T_e = 2$ keV. The yellow-shaded region indicates scale lengths characteristic of OMEGA experiments, while the blue-shaded region indicates scale lengths for ignition-scale designs.

the expected growth rate [Eq. (1)] and can be simply generalized to the case of multiple EM plane-wave irradiation.[22,24] A similar analysis can be performed including a linear variation in density δN. This results in the same two coupled differential equations (in wave-number space) that have been shown by Simon *et al*. to lead to the approximate threshold condition of Eq. (9) [e.g., Eqs. (3) and (4) in Simon *et al*.[6]].

Equation (4) can be used to compute the properties of linear stability with the combined effect of a density gradient and LW collisional damping, which are described by the terms δN and ν_e in Eq. (4), respectively, together with the effects of multibeam irradiation through the boundary conditions applied to Eq. (3). Figure 134.35 shows the numerically determined absolute threshold containing both LW dissipation and plasma inhomogeneity by solving Eq. (4) for two overlapped plane EM waves (see Fig. 134.36). A more-complete stability analysis must take into account the geometry and polarization of laser irradiation for a given experiment[24]—a three-dimensional

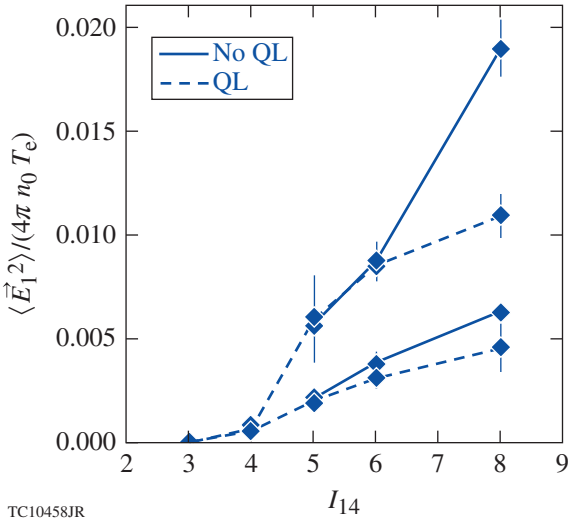

Figure 134.36
The electrostatic field intensity $\langle | \vec{E}_1 |^2 \rangle / (4\pi n_0 T_e)$ at nonlinear saturation as a function of laser intensity for a plasma with $Z_{eff} = 14$, $L_n = 330\ \mu$m, and $T_e = 2$ keV. The dashed (solid) curves show the results with (without) quasi-linear (QL) evolution of the electron-distribution function. The upper and lower sets of two curves correspond to strong $(\tilde{\nu}_i = 0.1)$ and weak $(\tilde{\nu}_i = 0.02)$ IAW damping, respectively. The error bars indicate the root-mean-square (rms) deviation from the average value at saturation.

problem. Currently, this is being investigated using a new code (*ZAK3D*) that solves Eqs. (4) and (5) in three dimensions.[75,76]

For ignition-class lasers with ~1 MJ of laser energy [e.g., the National Ignition Facility (NIF)[77]], the TPD threshold in direct-drive designs[37] is exceeded by a wider margin than in experiments on OMEGA/OMEGA EP, not because of a significant increase in laser intensity but because of the 2× to 3× increase in density scale length. As can be seen in Fig. 134.35, the inhomogeneity threshold is decreased by roughly a factor of 2 to 3. For such scale lengths, the collisional threshold can be made comparable to the inhomogeneity threshold by increasing the effective ionization state $Z_{eff} \equiv \langle Z^2 \rangle / \langle Z \rangle$ of the ablator material to $Z_{eff} \sim 14$ (e.g., silicon) (for multiple ion-species plasmas, the effective electron–ion collision frequency is obtained by replacing $Z \longrightarrow Z_{eff}$ in the usual expression for ν_{ei}). From the point of stability with respect to TPD, Fig. 134.35 suggests that increasing the Z_{eff} of the ablator is beneficial (for a fixed electron temperature), particularly if TPD is marginally unstable in CH, since satisfactory mid-Z ablators can be designed.[35,36]

All calculations presented in **Nonlinear Saturation** (p. 118) have assumed that the electromagnetic pump consisted of two plane EM waves incident at angles of ±23° with respect to the direction of the density gradient (see Fig. 134.37). The plasma parameters were chosen to be those of recent long-scale-length experiments in CH targets.[16,65] When Z_{eff} was varied, these hydrodynamic parameters were not changed: the electron temperature was $T_e = 2$ keV with $T_i = 1.5$ keV for ions. The density scale length was $L_n = 330\ \mu$m with the simulation box length L_x set to include densities from 0.19 n_c to 0.27 n_c, i.e. $L_x = (8/23)\, L_n$. [A separate analysis based on radiation–hydrodynamic simulations has been used to calculate the dependence of plasma parameters (e.g., density scale length and electron temperature) at the quarter-critical surface for different ablator materials with similar irradiation conditions[34] but this will not be discussed here.] When simulating a multiple-ion-species plasma, Eq. (5) was used to simulate an "effective" IAW such that Z and m_i were replaced by their averages (over ion species) except in the collisional LW damping rate as mentioned previously. Values of $Z_{eff} = 5.3$, 10, and 14 were obtained by modeling CH, SiO_2, and Si plasmas, respectively. The IAW damping rate ν_i is currently a fixed parameter that is initialized at the start of the calculation. This was equated with the expected Landau-damping rate of the least-damped IAW mode[78,79] for CH, SiO_2, and Si, except for the $Z_{eff} = 10$ and 14 strong damping cases, where $\tilde{\nu}_i$ was set to $\tilde{\nu}_i = 0.1$, where $\tilde{\nu}_i \equiv \nu_i / \omega_s$ is the dimensionless IAW damping rate and $\omega_s \simeq k c_s$ is the IAW frequency.

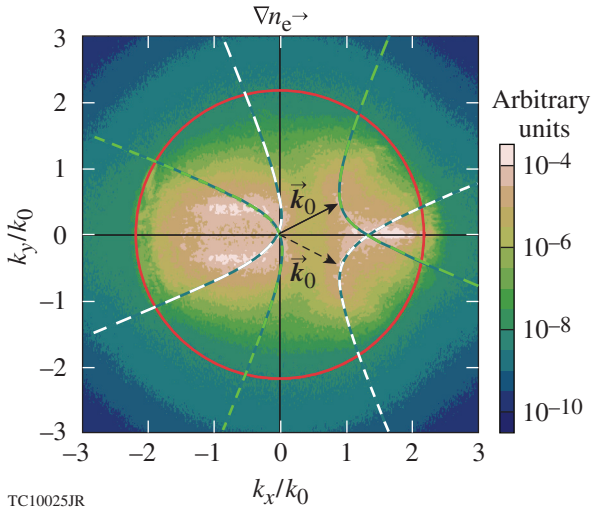

Figure 134.37
The time-averaged electrostatic field spectrum $\langle | \vec{E}_1(\vec{k}) |^2 \rangle_\tau$ (in arbitrary units) taken from a representative run at a time when nonlinear saturation has been attained. The instability is driven by two plane EM waves (black arrows) that are incident at an angle of ±23° with respect to the direction of the density gradient (x direction) and are polarized in the simulation (x,y) plane. The green (white) curves show the location of the maximum in growth rate as calculated by homogeneous theory [Eq. (1)]. The red circle indicates the location of the Landau cutoff $(| \vec{k} | \lambda_{De} = 0.25)$.

For non-negligible LW amplitudes, the *QZAK* model includes nonlinear coupling to ion fluctuations δn, which introduces a rich variety of nonlinear and turbulent phenomena. It also includes quasi-linear (kinetic) effects. Together, these effects will determine the long-time behavior of TPD relevant to experiment and the relative importance between absolute modes and convective modes in the nonlinear state.

Nonlinear Saturation

1. Anomalous Absorption
   (Heating of Near-Thermal Electrons)

Several diagnostics have been implemented to quantify the level of two-plasmon–decay instability and its dependence on plasma composition. Figure 134.37 shows the spatially averaged Langmuir-wave intensity $\left\langle \left| \vec{E}_1 \right|^2 \right\rangle \Big/ 4\pi n_0 T_e$ as a function of laser intensity for $Z_{eff} = 14$ at late time, when $\left\langle \left| \vec{E}_1 \right|^2 \right\rangle$ is judged to be steady. In all cases, spatial averaging is carried out over the whole simulation box that spans initial densities from 0.19 n_c to 0.27 n_c. It is convenient to define the energy (per unit length in the ignorable coordinate z) associated with electrostatic

$$W_1(t) \equiv \int \mathrm{d}x\mathrm{d}y \left| \vec{E}_1(x,y,t) \right|^2 \Big/ (4\pi)$$

and electromagnetic waves

$$W_2(t) \equiv \int \mathrm{d}x\mathrm{d}y \left| \vec{E}_2(x,y,t) \right|^2 \Big/ (8\pi)$$

[which are simply related to the above spatial averages

$$W_1 = A\left\langle \left| \vec{E}_1 \right|^2 \right\rangle \Big/ (4\pi),\ W_2 = A\left\langle \left| \vec{E}_2 \right|^2 \right\rangle \Big/ (8\pi),$$

where $A = L_x \times L_y$ is the area of the simulation box]. The effect of the quasi-linear evolution of the distribution function can be seen by comparing the saturated level of $\left\langle \left| \vec{E}_1 \right|^2 \right\rangle \Big/ 4\pi n_0 T_e$ with and without evolution of Eq. (6) for the spatially averaged electron-distribution function. Previously in Myatt *et al.*,[26] estimates of electron heating by TPD were based on the *ZAK* model using test particles; Fig. 134.37 demonstrates the importance of self-consistently evolving the electron-distribution function. The results are broadly consistent with those anticipated.[26] Figure 134.38 shows a contour plot of the self-consistently evolved electron-distribution function, where significant deviation from the initial Maxwellian distribution is evident.

Figure 134.39 illustrates the dependence of $\left\langle \left| \vec{E}_1 \right|^2 \right\rangle \Big/ 4\pi n_0 T_e$ (or equivalently W_1) on laser intensity for three values of Z_{eff} (5.3, 10, and 14) and for weak $\left(\tilde{\nu}_i = 0.02\right)$ and strong $\left(\tilde{\nu}_i = 0.1\right)$ ion-acoustic damping. It is evident that for a given ion-acoustic damping rate, the case of $Z_{eff} = 14$ has the lowest value of W_1. Regardless of the value of Z_{eff}, W_1 is smaller if ion-acoustic waves are weakly damped. The saturated value of W_1 can be connected to enhanced absorption of laser energy in the quarter-critical region in the following way: it can be shown

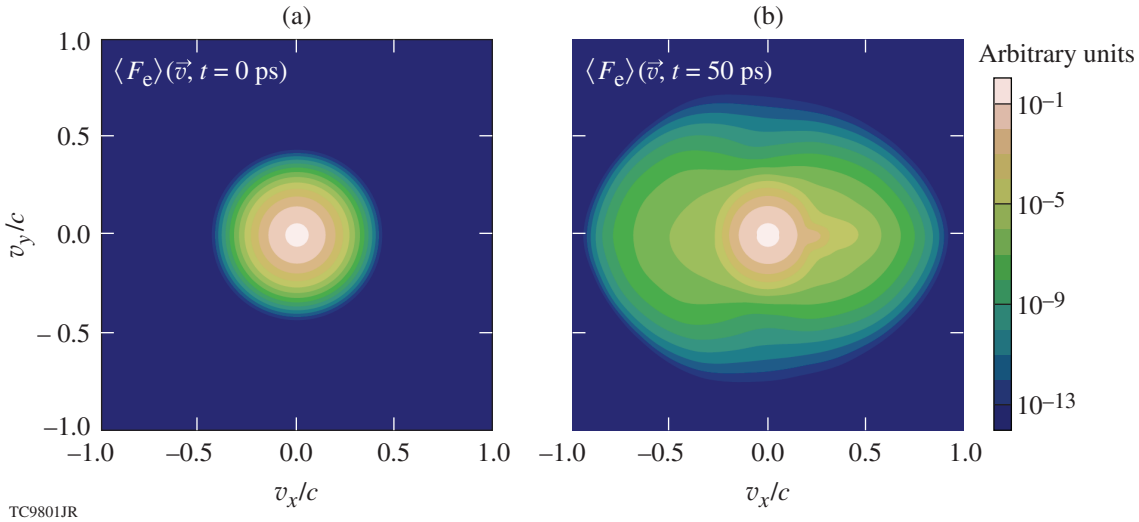

Figure 134.38
The electron distribution function $\left\langle F_e \right\rangle (\vec{v}, t = 0)$ is shown in velocity space at (a) $t = 0$ ps and (b) at a later time ($t = 50$ ps) after evolving according to the self-consistent quasi-linear diffusion equation [Eq. (6)].

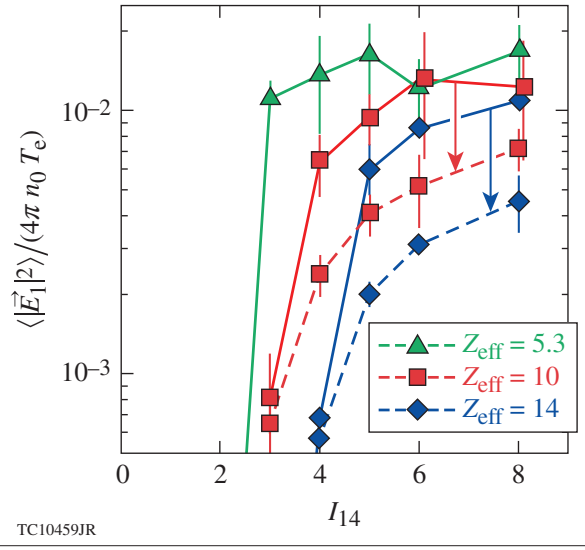

Figure 134.39
The electrostatic field intensity $\langle|\vec{E}_1|^2\rangle/(4\pi n_0 T_e)$ at nonlinear saturation as a function of total laser intensity for values of Z_{eff} = 5.3 (green), 10 (red), and 14 (blue), and for weak $(\tilde{\nu}_1 = 0.02)$ (dashed) and strong $(\tilde{\nu}_1 = 0.1)$ ion-acoustic wave (IAW) damping (solid curves). The error bars give the rms deviation from the mean values. The deviation can become quite significant for the most strongly driven cases.

that the field equations [Eqs. (3)–(5)] satisfy the energy conservation law

$$\partial_t\left[W_1 + W_2\right] = -2\sum_k\left[\nu_{coll} + \gamma_L(\vec{k})\right]\frac{\left|\vec{E}_1(\vec{k})\right|^2}{4\pi} - 2\nu_{2,T}W_2 - \int d\vec{s}\cdot\vec{\mathcal{P}}_2, \tag{10}$$

where $\vec{\mathcal{P}}_2$ is the Poynting vector

$$\vec{\mathcal{P}}_2 = \left(c^2/4\omega_p\right) i\left[\vec{E}_2^{\,*}\cdot\nabla\vec{E}_2 - \vec{E}_2\cdot\nabla\vec{E}_2^{\,*}\right]$$

and recalling that $\nu_{2,T} \approx \left(n_0/n_c\right)\nu_{ei}/2$ is the damping rate of the driving EM waves and $\nu_{coll} \approx \nu_{ei}/2$. Note that the dissipation associated with ion-acoustic waves does not enter in Eq. (10) because of the smallness of the mass ratio. In statistical steady state, defined by $\langle\partial_t[W_1 + W_2]\rangle_\tau = 0$, where $\langle\,\rangle_\tau$ implies a running time average,

$$-\left\langle\int d\vec{s}\cdot\vec{\mathcal{P}}_2\right\rangle_\tau = \frac{\nu_{ei}}{4}\left[1 + 4\frac{\langle W_1\rangle_\tau}{\langle W_2\rangle_\tau}\right]\langle W_2\rangle_\tau + 2\sum_k\left\langle\gamma_L(\vec{k})\frac{\left|\vec{E}_1(\vec{k})\right|^2}{4\pi}\right\rangle_\tau, \tag{11}$$

which, if $\gamma_L(\vec{k})$ is positive definite, gives the lower bound for the amount of power dissipated in the quarter-critical region, caused by electron–ion collisions, by the incident electromagnetic waves:

$$-\left\langle\int d\vec{s}\cdot\vec{\mathcal{P}}_2\right\rangle_\tau \gtrsim \frac{\nu_{ei}}{4}\left[1 + 4\frac{\langle W_1\rangle_\tau}{\langle W_2\rangle_\tau}\right]\langle W_2\rangle_\tau. \tag{12}$$

The term in the square brackets in Eq. (12) is a factor that multiplies the usual collisional energy absorption rate. This factor represents the anomalous (anom) enhancement of laser energy absorption caused by TPD $\eta_{anom} \equiv 1 + 4\langle W_1\rangle_\tau/\langle W_2\rangle_\tau$ (the assumption being that absorption is caused by electron–ion collisions and does not involve suprathermal electrons). A value of η_{anom} = 1 would give the usual amount of power dissipated that is associated with collisional absorption of light waves and corresponds to the usual terms present in ICF direct-drive hydrodynamic design codes. This can be estimated, for small absorption, as $(I_0 - I)/I_0 \approx \left(\nu_{ei}/4\right)\left(L_x/c\right) \sim 0.24$ (for CH). Figure 134.40 shows Fig. 134.39 replotted to illustrate the dependence of η_{anom} on laser intensity for materials of different ionization Z_{eff} and IAW damping rate. These results could be used to modify hydrocode predictions in a simple way by introducing a multiplier (η_{anom}) on the usual inverse bremsstrahlung term.

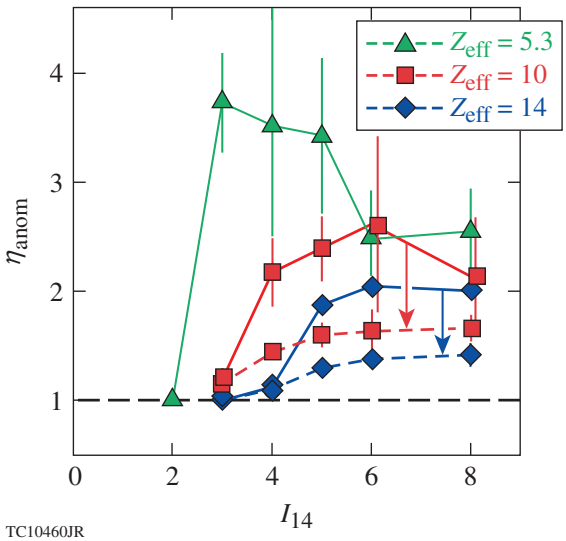

Figure 134.40
The anomalous absorption factor η_{anom} [see Eq. (12)] computed as a function of total laser intensity for values of Z_{eff} = 5.3 (green), 10 (red), and 14 (blue), for weak $(\tilde{\nu}_1 = 0.02)$ (dashed) and strong $(\tilde{\nu}_1 = 0.1)$ IAW damping (solid curves). The error bars show the rms deviation from the mean value computed at nonlinear saturation.

Figure 134.41 shows the dissipation spectrum

$$\left\langle \gamma_{\mathrm{L}}(\vec{k}) \left| \vec{E}_1(\vec{k}) \right|^2 \Big/ (4\pi) \right\rangle_{\tau}$$

that is associated with suprathermal electron production, i.e., the last term on the right-hand side of Eq. (11). It can be seen that features similar to the linearly unstable LW's exist, but dissipation extends to the Landau cutoff. Comparison of the size of the two terms on the right-hand side of Eq. (11) shows that the first (collisional term) is generally larger than the second, and that pump depletion is important for the more strongly driven runs presented here. It also suggests that the reference electron temperature T_{e} should be evolved. A future improvement of the code will be to evolve Eq. (3) self-consistently including pump depletion and collisional absorption. Evolution of the reference electron temperature T_{e} will also be considered.

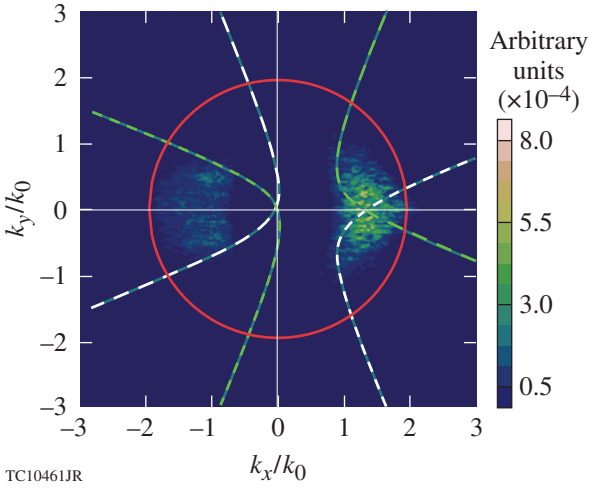

Figure 134.41
A snapshot of the dissipation spectrum $\gamma_{\mathrm{L}}(\vec{k}) \left| \vec{E}_1(\vec{k}) \right| / (4\pi)$ (in arbitrary units) that is associated with hot-electron generation and whose sum determines the power dissipated by collisionless processes [Eq. (11)]. As in Fig. 134.36, the green (white) curves show the spectral location of the maximum in TPD growth rate as calculated by homogeneous theory for each beam [Eq. (1)] and the red circle indicates the location of the Landau cutoff $\left(\left| \vec{k} \right| \lambda_{\mathrm{De}} = 0.25 \right)$.

2. The Production of Energetic Electrons

Velocity moments can be taken of Eq. (6) in the usual way to obtain evolution equations for the hydrodynamic variables. For example, an energy equation can be derived from Eqs. (6) and (7) for the spatially averaged electron-distribution function $\langle F_{\mathrm{e}} \rangle$ (by multiplying by $m_{\mathrm{e}} v^2/2$ and integrating over velocities) with the result

$$\partial_t W_{\mathrm{e}} + A \sum_{i=1}^{2} \frac{s_i}{L_i} \Delta Q_i = \sum_k \gamma_k \frac{\left| \vec{E}(\vec{k}) \right|^2}{16\pi} + \int \mathrm{d}\vec{v} \, \frac{1}{2} m v^2 \hat{\sigma}_{\mathrm{IB}} \left[\left\langle F_{\mathrm{e}} \right\rangle, \left| \vec{E}_1 \right|^2 \right] + \int \mathrm{d}\vec{v} \, \frac{1}{2} m v^2 \hat{\sigma}_{\mathrm{IB}} \left[\left\langle F_{\mathrm{e}} \right\rangle, \left| \vec{E}_{2,T} \right|^2 \right], \qquad (13)$$

where $W_{\mathrm{e}} = \left(m_{\mathrm{e}} / 2 \right) \int \mathrm{d}\vec{v} v^2 \left\langle F_{\mathrm{e}} \right\rangle$ is the total electron kinetic energy. The terms on the right-hand side of Eq. (13) can be identified as the dissipated power associated with the production of suprathermal electrons, the collisional absorption of Langmuir waves, and collisional absorption of the pumping laser (which is usually the only term included in radiation–hydrodynamic calculations). A statistical steady state can exist if these source terms balance the flux through the boundaries, where $\Delta Q_i \equiv \Delta Q_i^{>} - \Delta Q_i^{<} = \left(q_i^{>} - q_{i,0}^{>} \right) - \left(q_i^{<} - q_{i,0}^{<} \right)$ and the subscript i denotes each of the coordinate directions. The heat flux has its usual definition $\vec{q} \equiv \left(m_{\mathrm{e}} / 2 \right) \int_0^{\infty} \mathrm{d}\vec{v} \vec{v} v^2 \left\langle F_{\mathrm{e}} \right\rangle$ with the exception that the integral is split into two parts $q_i = q_i^{<} + q_i^{>}$, depending on the sign of the velocity component v_i [i.e., each piece corresponds to either forward-going (>) or backward-going (<) velocities with respect to the i direction]. The subscript "0" implies that it is calculated with the initial electron-distribution function $\langle F_{\mathrm{e}} \rangle (t = 0)$. For a symmetric (e.g., Maxwellian) initial distribution, $\vec{q}_0^{\,>} = -\vec{q}_0^{\,<}$ and the net heat flux vanishes.[80]

Together with Eq. (10), global energy conservation may be expressed as

$$\partial_t \left[W_1 + W_2 + W_{\mathrm{e}} \right] = -A \sum_{i=1}^{2} \frac{s_i}{L_i} \Delta Q_i - \int \mathrm{d}\vec{s} \cdot \vec{\mathcal{P}}_2 \qquad (14)$$

provided that

$$\int \mathrm{d}\vec{v} (1/2) m v^2 \hat{\sigma}_{\mathrm{IB}} \left[\left\langle F_{\mathrm{e}} \right\rangle, \left| \vec{E}_1 \right|^2 \right]$$

can be reduced to $\nu_{\mathrm{ei}} \langle W_1 \rangle$ and

$$\int \mathrm{d}\vec{v} (1/2) m v^2 \hat{\sigma}_{\mathrm{IB}} \left[\left\langle F_{\mathrm{e}} \right\rangle, \left| \vec{E}_{2,T} \right|^2 \right]$$

to $2\nu_{2,T} \langle W_2 \rangle \sim \nu_{\mathrm{ei}} \langle W_{2,T} \rangle / 4$. Therefore, in statistical steady state

$$-\frac{1}{A} \left\langle \int \mathrm{d}\vec{s} \cdot \vec{\mathcal{P}}_2 \right\rangle_{\tau} = \sum_{i=1}^{2} \frac{s_i}{L_i} \left\langle \Delta Q_i \right\rangle_{\tau}, \qquad (15)$$

and the absorbed power of the laser is balanced by the power flowing through the boundaries carried by the kinetic energy of electrons. For the case where the velocity space diffusion is assumed periodic in the i direction (which is the y direction transverse to the density gradient in all the calculations presented here), the corresponding flux term $\Delta Q_i / L_i$ is absent. Consequently, for doubly periodic boundaries, the only steady-state solution is the trivial one $\left\langle \int d\vec{s} \cdot \vec{\mathcal{P}}_2 \right\rangle_\tau = 0$. When one boundary is open (e.g., in the direction of the gradient), it corresponds to the use of "thermalizing" boundaries as is often implemented in PIC codes. The applicability of these boundary conditions has been discussed in Myatt *et al.*,[26] where the possibility of the reheating of electrons that pass multiple times through the quarter-critical region was evaluated.

Figure 134.42 shows the hot-electron power fraction $f_h^{>30}$ as a function of time for two runs that correspond to overlapped laser intensities of $I_L = 6 \times 10^{14}$ W/cm^2 and an effective ionization of $Z_{eff} = 10$ for two values of the ion-acoustic damping rate ($\tilde{\nu}_i = 0.1$ and 0.02). The fraction $f_h^{>30}(t)$ is defined as the ratio of the heat flux ΔQ_x to the (constant) laser intensity I_L (in W/cm^2) with the restriction that the limits on the range of integration in the integral determining the heat flux ΔQ_x are adjusted to include only electrons having energies greater than 30 keV (for this reason, the superscript). Experimentally, the fraction $f_{h,exp} \equiv E_h / E_L$ is a time-integrated measurement often determined (for a laser pulse of energy E_L) by inferring the energy E_h of suprathermal electrons via the strength of K_α emission from a fluorescent layer buried in the target.[16] A model of electron–photon transport in matter is used to relate the observed energy in K_α emission to the energy of hot electrons. For example, a molybdenum layer was used in Yaakobi *et al.*[16] having $E_{K_\alpha} \approx 17.5$ keV [which justifies our cutoff energy of 30 keV in the definition of $f_h^{>30}(t)$]. To facilitate a comparison with experiment, we define a running time average $\langle f_h^{>30} \rangle_\tau$. It can be seen from Fig. 134.42 that it is often possible to define a meaningful steady state so that $\langle f_h^{>30} \rangle_\tau$ is constant (and can be crudely equated with the experimental energy fraction $\langle f_h^{>30} \rangle_\tau \sim f_{h,exp}$). This steady-state time average (for $\tau > 35$ ps) is plotted in Fig. 134.43 for materials of varying Z_{eff} and $\tilde{\nu}_i$.

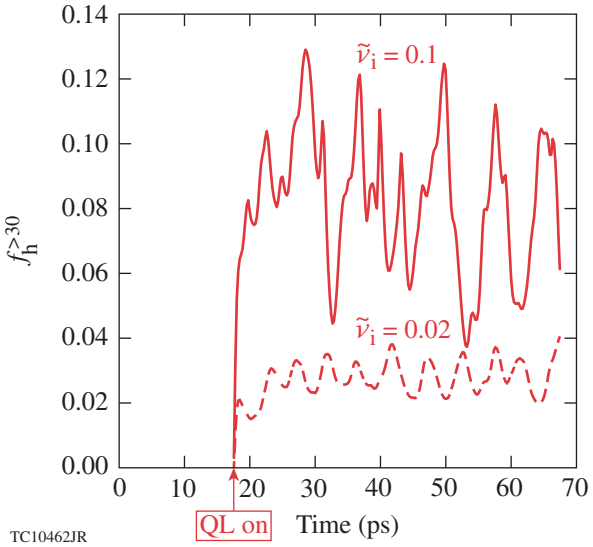

Figure 134.42
The heat flux carried by hot electrons with energies greater than 30 keV as a fraction of the incident laser power as a function of time $\left[f_h^{>30}(t)\right]$. These results were obtained for a plasma with $Z_{eff} = 10$ and a total laser intensity of 5×10^{14} W/cm^2. The solid curve corresponds to an ion-acoustic damping rate of $\tilde{\nu}_i = 0.1$, while the dashed curve corresponds to $\tilde{\nu}_i = 0.02$. In both cases, the runs commence at $t = 0$ but quasi-linear diffusion is not started until approximately $t = 17$ ps (as indicated by the arrow).

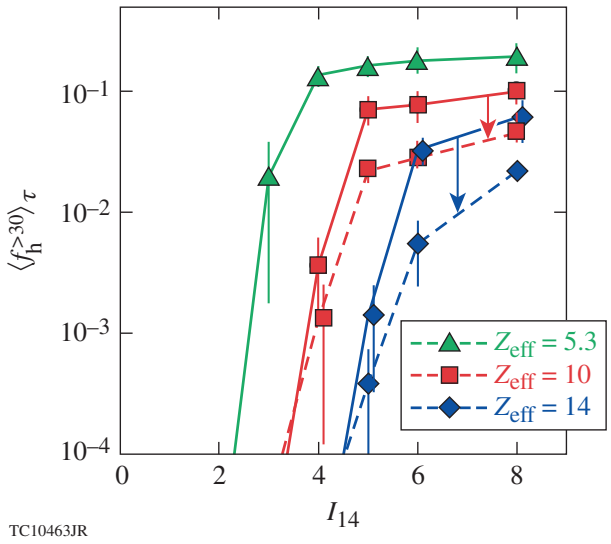

Figure 134.43
Hot-electron fraction $\langle f_h^{>30} \rangle_\tau$, as determined at nonlinear saturation as a function of total laser intensity for $Z_{eff} = 5.3$ (green curve), 10 (red curve), and 14 (blue curve). The solid curves indicate runs with an IAW damping rate of $\tilde{\nu}_i = 0.1$, while the dashed curves correspond to $\tilde{\nu}_i = 0.02$. The error bars quantify the rms fluctuations about the average that is associated with the steady state.

Figure 134.43 shows the main results of this study. It can be seen that the hot-electron fraction $\langle f_h^{>30} \rangle_\tau$ increases rapidly for $I_L \gtrsim 3$ to 5×10^{14} W/cm^2 (with a threshold depending on Z_{eff}) and then saturates at the level of several percent for CH targets, which is broadly consistent with PIC calculations[27,68] when electron–ion collisions are accounted for (in the RPIC calculations of Vu *et al.*,[27] grid damping plays the role of elec-

tron–ion collisions), and also experimental measurements[65] (the density scale length, electron temperature, and laser intensities were motivated by OMEGA EP experimental conditions using CH targets[65]). Calculations of SiO_2 targets, having weak ion-acoustic wave damping $\left(\tilde{\nu}_i = 0.02\right)$, show a similar intensity dependence but saturate at a level approximately half that of CH targets, while calculations of Si targets ($Z_{\text{eff}} = 14$, $\tilde{\nu}_i = 0.02$ had the lowest hot-electron fraction of all, which is particularly pronounced at mid-intensities ($I_L \sim 5 \times 10^{14}$ W/cm^2). In part, this is due to the effect of the increased threshold for Si associated with the Langmuir-wave damping (see Fig. 134.35).

In general, the lowest hot-electron production was seen for materials with the highest Z_{eff} and the smallest ion-acoustic wave damping $\tilde{\nu}_i = 0.02$. This suggests CH ablators might not be the best choice of ablator material from the point of view of TPD.

3. Confirmation of the Sensitivity to Ion-Acoustic Damping Using RPIC Calculations

Two 2-D RPIC simulations that do not make the quasi-linear approximation or any assumption regarding the spatial uniformity of the electron distribution function were performed to independently investigate the effect of the IAW damping rate on the development and saturation of TPD.

Over 50 *QZAK* calculations were performed in the current analysis, most for a long density scale length (L_n = 330 μm) and integrated out to times close to ~0.1 ns (~5 ns in combined total). Because RPIC calculations are much more computationally intensive than *QZAK*, the RPIC calculations were performed at a shorter scale length (L_n = 130 μm) and integrated for shorter times (t = 9 ps). The ion-acoustic damping rate was modified by varying the ion Landau-damping contribution to $\tilde{\nu}_i$ through the ion temperature [a hydrogen (Z = 1) plasma was assumed]. All other physical parameters were the same as described earlier for the *QZAK* calculations.

The two RPIC simulations used identical simulation domains consisting of 4096 (x direction) × 1024 (y direction) computational cells, and the electron and proton distributions were each represented by 32 particles/computational cell. The boundary conditions were compatible with those assumed by *QZAK* [see **Numerical Simulation of TPD Growth and Saturation in Inhomogeneous Collisional Plasma** (p. 113) and **The Production of Energetic Electrons** (p. 120)]: the particles were recycled periodically in the y direction and absorbed at the surfaces $x = 0$ (laser entrance boundary) and $x = L_x$ (laser exit boundary). At these boundaries, Maxwellian baths of electrons with temperature T_e and ions with temperature T_i were assumed, and the particles absorbed at these surfaces were replenished accordingly. Each of the two incident pump plane EM waves was given an intensity of $I_0 = 1 \times 10^{15}$ W/cm^2 with polarization in the x–y plane.

The so-called "low" and "high" IAW damping simulations correspond to $T_i = 0.1$ keV $\left(T_e/T_i = 20 \text{ and } \tilde{\nu}_i \approx 1.11 \times 10^{-3}\right)$ (electron Landau damping of IAW is not present in RPIC) and $T_i = 1$ keV $\left(T_e/T_i = 2 \text{ and } \tilde{\nu}_i \approx 2.70 \times 10^{-1}\right)$, respectively. The high-damping case has been presented elsewhere,[27,28] but the results are reproduced here for comparison. Figure 134.44 shows the suprathermal heat flux f_h ($\Delta Q_x^{>}$ normalized to the total laser intensity) as a function of time over a period of 10 ps for both cases. In the simulations, $\Delta Q_x^{>}$ is computed from the electron flux accumulated at the laser exit boundary ($x = L_x$) accounting for electrons of all energies. As before [**The Production of Energetic Electrons** (p. 120)], $\Delta Q_x^{>}$ represents the electron heat flux in excess of its initial (Maxwellian) value.

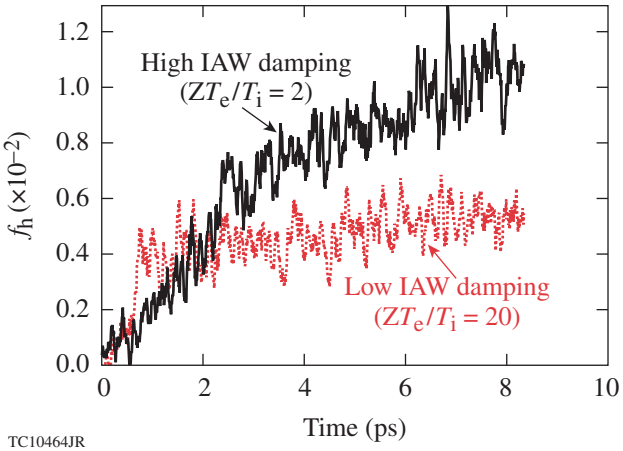

Figure 134.44
The suprathermal heat flux f_h, as computed by the code RPIC,[27] is shown as a function of time for cases of high $\left(\tilde{\nu}_i \approx 2.70 \times 10^{-1}\right)$ and low $\left(\tilde{\nu}_i \approx 1.11 \times 10^{-3}\right)$ IAW damping. While the low-damping case reaches saturation much more quickly, its saturation level is lower.

Figure 134.44 indicates that both the high-damping and low-damping cases reached saturation, and that the high-damping case achieved a suprathermal heat flux $\Delta Q_x^{>}$ about twice as large as that of the low-damping case. Furthermore, while the high-damping case took several (~10) picoseconds to reach saturation, the low-damping case achieved saturation in about

0.5 ps. The comparison shown in Fig. 134.44 presents supporting evidence that the IAW damping rate has an important effect on the temporal development and saturation level of TPD.

The RPIC simulation corresponding to high $\tilde{\nu}_i$ and shown in Fig. 134.44 has been previously analyzed in some detail.[27,28] The nonlinear state was described in terms of cavitating LW turbulence, and it was determined that prerequisites for the quasi-linear description were met—i.e., the distribution function was well described by its spatial average and trapping effects were negligible.[28] A comparison between RPIC and *QZAK* is given in Vu *et al.*,[81] but we speculate here on the importance of the ion-acoustic damping rate in the context of cavitating LW turbulence.

4. Dependence of $\langle f_h \rangle$ on the IAW Damping Rate and Nucleation Dynamics

The significant sensitivity of the saturated level of TPD excitation on the IAW damping rate is clearly a nonlinear effect since the linear theory does not involve IAW's. Such sensitivity might be anticipated since it has been observed in previous *ZAK* model studies of SRS in the weak Landau-damping regime.[29] Previous work[30–32] has also demonstrated that nucleation of cavitons is favored by strong IAW damping. The detailed manifestation of this for the simulation regime considered here is under study. A qualitative summary of our current view is based on the assumption that Langmuir cavitation and collapse are the dominant processes in the nonlinear stage of TPD for the parameters considered.[28]

In the cavitating turbulence scenario, the level of electrostatic fluctuations is governed by the nucleation–collapse–burnout cycle[82,83] and the time scale of this process is governed by the IAW damping rate.[27] The interference pattern of the linearly excited triad of free plane LW's (see Fig. 134.36) produces density trenches that are modulated longitudinally by the beating of the forward common LW with the backward pair of triad waves. The ponderomotive force from the peaks in $\left|\vec{E}_1\right|^2$ resulting from this modulation produces density depressions that can support localized (or bound) states of the Langmuir field. The backward triad waves have long wavelengths and frequencies near the local electron plasma frequency and can directly nucleate the bound state.[82,83] These localized states then proceed to collapse and burn out, producing a large enhancement of LW energy and electron flux. As the triad modes evolve to higher k values,[28] the spatial scale of the longitudinal modulation appears to produce much stronger, smaller-scale density cavities in the trenches. These residual cavities appear to be too narrow and deep to efficiently nucleate new cavitons. The Langmuir turbulence then dies out locally until the short-scale density fluctuations dissipate by IAW Landau damping. The nucleation process can then resume with another burst of Langmuir turbulence once this has occurred.

In the nucleation–collapse–burnout cycle,[82,83] a source must be present that can excite the bound state. The nucleation source is essentially the overlap integral of the bound-state wave function and the source, which may be the TPD current on the right-hand side of Eq. (4). This source produces freely propagating LW's that are dominantly the triad modes discussed recently.[27,28] If this source has frequencies close enough to the bound-state eigenfrequency, it can cause a near-resonant excitation of the bound state and initiate a collapse. To have such frequencies, free LW's must have long wavelengths such that the bound-state wave function having the largest overlap integral with this long-wavelength source is the lowest or "ground state" with no nodes in its wave function. Our experience is that only this state is appreciably excited. A density well that is too deep may have a deeply bound ground-state wave function, which will not efficiently couple to a long-wavelength free LW. This means that for efficient nucleation, the density well should not be too deep, implying that the spatial width should be large enough to trap a weakly bound ground state. Strong IAW damping appears to produce more cavities of this type (because of this nucleation effect, the LDI cascade, where LW's decay into LW's with increasingly lower wavelengths, never progresses past a few steps before cavitons are nucleated in the ion-density fluctuations created by the LDI process itself).[29] For these TPD simulations, LDI appears to play a minor role, while the TPD triad[25] and the ion-density fluctuations arising from their beating play a similar role in the nucleation process.

It is very difficult to diagnose, in microscopic detail, a system with as many as 10^4 cavitons.[28] The scenario outlined above is consistent with our experience with simpler systems. Further microscopic details will be presented in a future publication.

Summary and Discussion

A two-dimensional model that further generalizes the extended Zakharov model of TPD to include quasi-linear diffusion of the electron distribution function has been described. The model addresses the nonlinear evolution of the TPD instability caused by the self-consistent coupling of TPD-generated LW's with ion-density fluctuations and quasi-linear evolution of the electron-distribution function. Quasi-linear evolution of

the electron-distribution function was shown to lead to saturation of the average LW intensity at lower values than predicted by the Zakharov model alone for parameters of interest to recent experiments.

In the linear regime of infinitesimal LW amplitude, the model allows for TPD stability to be determined in the presence of both density inhomogeneity and LW damping for a laser pump described in terms of multiple overlapping plane EM waves in two dimensions. A more-complete treatment requires the model to be solved in three dimensions. A 3-D code solving Eqs. (4) and (5) but omitting the quasi-linear diffusion terms is described in Zhang *et al*.[76] It was shown that collisional damping of LW's is important for directly driven ICF targets at the ignition scale. In the nonlinear stage of TPD it was shown that the energy absorbed by the target and converted into electron thermal energy by the collisional absorption of TPD LW's is comparable to, or greater than, the energy converted into hot electrons. It was suggested that maximizing the collisional damping of LW's in direct-drive designs could be beneficial in mitigating TPD absorption and preheat.

For fixed electron temperature and density scale length, the lowest hot-electron production was seen for materials with the highest Z_{eff} and the smallest IAW damping rate. The reduction in hot-electron fraction can be partly explained by the increased threshold. The nonlinear effect associated with weakly damped ion-acoustic waves was independently investigated with RPIC calculation, and a possible physical explanation for this effect was given in terms of nucleation dynamics of cavitating Langmuir turbulence. An experimental test might be to compare TPD in two materials of similar Z_{eff}, e.g., Si- and Ge-doped plastic, where the second material has a greater IAW damping rate because of the presence of light (H) ions.

Future improvements to the *QZAK* model will include implementation of terms describing the effects of pump depletion and collisional absorption for the EM pump. Self-consistent evolution of the reference electron temperature will also be investigated. Work is also underway to implement the quasi-linear diffusion equation in three dimensions.

ACKNOWLEDGMENT

This work was supported by the U.S. Department of Energy Office of Inertial Confinement Fusion under Cooperative Agreement No. DE-FC52-08NA28302, the University of Rochester, and the New York State Energy Research and Development Authority. The support of DOE does not constitute an endorsement by DOE of the views expressed in this article.

REFERENCES

1. M. V. Goldman, Ann. Phys. **38**, 117 (1966).
2. M. N. Rosenbluth, Phys. Rev. Lett. **29**, 565 (1972).
3. Y. C. Lee and P. K. Kaw, Phys. Rev. Lett. **32**, 135 (1974).
4. V. P. Silin and A. N. Starodub, Sov. Phys.-JETP **39**, 82 (1974).
5. A. B. Langdon, B. F. Lasinski, and W. L. Kruer, Phys. Rev. Lett. **43**, 133 (1979).
6. A. Simon, R. W. Short, E. A. Williams, and T. Dewandre, Phys. Fluids **26**, 3107 (1983).
7. H. Derblom *et al*., J. Geophys. Res, A, Space Phys. **94**, 10111 (1989).
8. D. W. Phillion *et al*., Phys. Rev. Lett. **49**, 1405 (1982).
9. W. Seka, R. E. Bahr, R. W. Short, A. Simon, R. S. Craxton, D. S. Montgomery, and A. E. Rubenchik, Phys. Fluids B **4**, 2232 (1992).
10. S. P. Regan, N. B. Meezan, L. J. Suter, D. J. Strozzi, W. L. Kruer, D. Meeker, S. H. Glenzer, W. Seka, C. Stoeckl, V. Yu. Glebov, T. C. Sangster, D. D. Meyerhofer, R. L. McCrory, E. A. Williams, O. S. Jones, D. A. Callahan, M. D. Rosen, O. L. Landen, C. Sorce, and B. J. MacGowan, Phys. Plasmas **17**, 020703 (2010).
11. W. Seka, D. H. Edgell, J. F. Myatt, A. V. Maximov, R. W. Short, V. N. Goncharov, and H. A. Baldis, Phys. Plasmas **16**, 052701 (2009).
12. N. A. Ebrahim *et al*., Phys. Rev. Lett. **45**, 1179 (1980).
13. H. A. Baldis and C. J. Walsh, Phys. Rev. Lett. **47**, 1658 (1981).
14. D. M. Villeneuve, R. L. Keck, B. B. Afeyan, W. Seka, and E. A. Williams, Phys. Fluids **27**, 721 (1984).
15. C. Rousseaux *et al*., Phys. Fluids B **4**, 2589 (1992).
16. B. Yaakobi, P.-Y. Chang, A. A. Solodov, C. Stoeckl, D. H. Edgell, R. S. Craxton, S. X. Hu, J. F. Myatt, F. J. Marshall, W. Seka, and D. H. Froula, Phys. Plasmas **19**, 012704 (2012).
17. C. S. Liu and M. N. Rosenbluth, Phys. Fluids **19**, 967 (1976).
18. B. B. Afeyan and E. A. Williams, Phys. Rev. Lett. **75**, 4218 (1995).
19. E. Z. Gusakov, Sov. J. Plasma Phys. **8**, 324 (1982).
20. G. Laval, R. Pellat, and D. Pesme, Phys. Rev. Lett. **36**, 192 (1976).
21. C. Stoeckl, R. E. Bahr, B. Yaakobi, W. Seka, S. P. Regan, R. S. Craxton, J. A. Delettrez, R. W. Short, J. Myatt, A. V. Maximov, and H. Baldis, Phys. Rev. Lett. **90**, 235002 (2003).
22. D. F. DuBois, B. Bezzeridels, and H. A. Rose, Phys. Fluids B **4**, 241 (1992).
23. R. W. Short, Bull. Am. Phys. Soc. **53**, 245 (2008).

24. D. T. Michel, A. V. Maximov, R. W. Short, S. X. Hu, J. F. Myatt, W. Seka, A. A. Solodov, B. Yaakobi, and D. H. Froula, Phys. Rev. Lett. **109**, 155007 (2012).

25. H. X. Vu, D. F. DuBois, D. A. Russell, and J. F. Myatt, Phys. Plasmas **17**, 072701 (2010).

26. J. F. Myatt, J. Zhang, J. A. Delettrez, A. V. Maximov, R. W. Short, W. Seka, D. H. Edgell, D. F. DuBois, D. A. Russell, and H. X. Vu, Phys. Plasmas **19**, 022707 (2012).

27. H. X. Vu, D. F. DuBois, J. F. Myatt, and D. A. Russell, Phys. Plasmas **19**, 102703 (2012).

28. H. X. Vu, D. F. DuBois, D. A. Russell, and J. F. Myatt, Phys. Plasmas **19**, 102708 (2012).

29. D. A. Russell, D. F. DuBois, and H. A. Rose, Phys. Plasmas **6**, 1294 (1999).

30. D. F. DuBois *et al*., Phys. Fluids B **5**, 2616 (1993).

31. D. F. Dubois *et al*., J. Geophys. Res. **98**, 17543 (1993).

32. D. F. DuBois, D. A. Russell, and H. A. Rose, Phys. Rev. Lett. **74**, 3983 (1995).

33. V. A. Smalyuk, R. Betti, J. A. Delettrez, V. Yu. Glebov, D. D. Meyerhofer, P. B. Radha, S. P. Regan, T. C. Sangster, J. Sanz, W. Seka, C. Stoeckl, B. Yaakobi, J. A. Frenje, C. K. Li, R. D. Petrasso, and F. H. Séguin, Phys. Rev. Lett. **104**, 165002 (2010).

34. S. X. Hu, D. T. Michel, D. H. Edgell, D. H. Froula, R. K. Follett, V. N. Goncharov, J. F. Myatt, S. Skupsky, and B. Yaakobi, Phys. Plasmas **20**, 032704 (2013).

35. R. Betti, R. Nora, M. Lafon, J. F. Myatt, and K. S. Anderson, Bull. Am. Phys. Soc. **57**, 154 (2012).

36. M. Lafon, R. Nora, and R. Betti, Bull. Am. Phys. Soc. **57**, 153 (2012).

37. V. N. Goncharov, T. C. Sangster, T. R. Boehly, S. X. Hu, I. V. Igumenshchev, F. J. Marshall, R. L. McCrory, D. D. Meyerhofer, P. B. Radha, W. Seka, S. Skupsky, C. Stoeckl, D. T. Casey, J. A. Frenje, and R. D. Petrasso, Phys. Rev. Lett. **104**, 165001 (2010).

38. V. E. Zakharov, Sov. Phys.-JETP **35**, 908 (1972).

39. A. Hasegawa, Phys. Rev. A **1**, 1746 (1970).

40. R. C. Davidson, *Methods in Nonlinear Plasma Theory* (Academic Press, New York, 1972).

41. P. A. Robinson, Rev. Mod. Phys. **69**, 507 (1997).

42. M. V. Goldman, Rev. Mod. Phys. **56**, 709 (1984).

43. P. Y. Cheung and A. Y. Wong, Phys. Rev. Lett. **55**, 1880 (1985).

44. A. Y. Wong and P. Y. Cheung, Phys. Rev. Lett. **52**, 1222 (1984).

45. B. Eliasson and B. Thidé, J. Geophys. Res, A, Space Phys. **113**, A02313 (2008).

46. D. A. Russell and D. F. DuBois, Phys. Rev. Lett. **86**, 428 (2001).

47. J. Briand *et al*., Phys. Fluids B **2**, 160 (1990).

48. J. C. Weatherall, Astrophys. J. **506**, 341 (1998).

49. A. Hanssen *et al*., J. Geophys. Res, A, Space Phys. **97**, 12,073 (1992).

50. D. F. DuBois, H. A. Rose, and D. Russell, Phys. Rev. Lett. **66**, 1970 (1991).

51. D. F. DuBois and M. V. Goldman, Phys. Rev. **164**, 207 (1967).

52. A third-harmonic envelope could be used to describe $3/2\omega_0$ emission, as in Ref. 46.

53. A. N. Starodub and M. V. Filippov, Sov. J. Plasma Phys. **5**, 610 (1979).

54. V. Yu. Bychenkov, V. P. Silin, and V. T. Tikhonchuk, Sov. J. Plasma Phys. **3**, 730 (1977).

55. R. L. Berger and L. V. Powers, Phys. Fluids **28**, 2895 (1985).

56. W. Seka, B. B. Afeyan, R. Boni, L. M. Goldman, R. W. Short, K. Tanaka, and T. W. Johnston, Phys. Fluids **28**, 2570 (1985).

57. V. E. Zakharov, in *Handbook of Plasma Physics*, edited by M. N. Rosenbluth and R. Z. Sagdeev, Volume 2: Basic Plasma Physics II, edited by A. A. Galeev and R. N. Sudan (Elsevier Science Publishers B.V., Amsterdam, 1984), Chap. 5.3, pp. 81–121.

58. P. Mounaix *et al*., Phys. Fluids B **3**, 1392 (1991).

59. J. Dawson and C. Oberman, Phys. Fluids **5**, 517 (1962).

60. A series of runs were performed to investigate the sensitivity of the saturated state (described in terms of LW excitation level and hot-electron flux) to the LW noise level. No significant difference was found when varying the intensity of LW noise over two orders of magnitude.

61. K. Y. Sanbonmatsu *et al*., Phys. Plasmas **7**, 2824 (2000).

62. B. Fornberg, *A Practical Guide to Pseudospectral Methods*, Cambridge Monographs on Applied and Computational Mathematics, Vol. 1 (Cambridge University Press, Cambridge, England, 1998).

63. O. Skjaeraasen, P. A. Robinson, and D. L. Newman, Phys. Plasmas **18**, 022103 (2011).

64. D. Peaceman and H. H. Rachford, Jr., J. Soc. Indust. Appl. Math. **3**, 28 (1955).

65. D. H. Froula, B. Yaakobi, S. X. Hu, P.-Y. Chang, R. S. Craxton, D. H. Edgell, R. Follett, D. T. Michel, J. F. Myatt, W. Seka, R. W. Short, A. Solodov, and C. Stoeckl, Phys. Rev. Lett. **108**, 165003 (2012).

66. R. Yan, A. V. Maximov, C. Ren, and F. S. Tsung, Phys. Rev. Lett. **103**, 175002 (2009).

67. R. Yan, A. V. Maximov, and C. Ren, Phys. Plasmas **17**, 052701 (2010).

68. R. Yan, C. Ren, J. Li, A. V. Maximov, W. B. Mori, Z. M. Sheng, and F. S. Tsung, Phys. Rev. Lett. **108**, 175002 (2012).

69. C. S. Liu, in *Advances in Plasma Physics*, edited by A. Simon and W. B. Thompson (Wiley-Interscience, New York, 1976), Vol. 6, pp. 167–174.

70. B. F. Lasinski and A. B. Langdon, Lawrence Livermore National Laboratory, Livermore, CA, Report UCRL-50021-77, 4-49 (1978).

71. T. R. Boehly, D. L. Brown, R. S. Craxton, R. L. Keck, J. P. Knauer, J. H. Kelly, T. J. Kessler, S. A. Kumpan, S. J. Loucks, S. A. Letzring, F. J. Marshall, R. L. McCrory, S. F. B. Morse, W. Seka, J. M. Soures, and C. P. Verdon, Opt. Commun. **133**, 495 (1997).

72. L. J. Waxer, D. N. Maywar, J. H. Kelly, T. J. Kessler, B. E. Kruschwitz, S. J. Loucks, R. L. McCrory, D. D. Meyerhofer, S. F. B. Morse, C. Stoeckl, and J. D. Zuegel, Opt. Photonics News **16**, 30 (2005); D. N. Maywar, J. H. Kelly, L. J. Waxer, S. F. B. Morse, I. A. Begishev, J. Bromage, C. Dorrer, J. L. Edwards, L. Folnsbee, M. J. Guardalben, S. D. Jacobs, R. Jungquist, T. J. Kessler, R. W. Kidder, B. E. Kruschwitz, S. J. Loucks, J. R. Marciante, R. L. McCrory, D. D. Meyerhofer, A. V. Okishev, J. B. Oliver, G. Pien, J. Qiao, J. Puth, A. L. Rigatti, A. W. Schmid, M. J. Shoup III, C. Stoeckl, K. A. Thorp, and J. D. Zuegel, J. Phys., Conf. Ser. **112**, 032007 (2008).

73. M. V. Goldman, Ann. Phys. **38**, 95 (1966).

74. W. L. Kruer, in *The Physics of Laser Plasma Interactions*, Frontiers in Physics, Vol. 73, edited by D. Pines (Addison-Wesley, Redwood City, CA, 1988).

75. J. Zhang, J. F. Myatt, A. V. Maximov, R. W. Short, D. F. DuBois, D. A. Russell, and H. X. Vu, Bull. Am. Phys. Soc. **57**, 299 (2012).

76. J. Zhang, J. F. Myatt, R. W. Short, A. V. Maximov, H. X. Vu, D. F. DuBois, and D. A. Russell, "Multibeam Two-Plasmon Decay from Linear Threshold to Nonlinear Saturation," to be published in Physical Review Letters.

77. W. J. Hogan, E. I. Moses, B. E. Warner, M. S. Sorem, and J. M. Soures, Nucl. Fusion **41**, 567 (2001); E. I. Moses, Fusion Sci. Technol. **54**, 361 (2008).

78. H. X. Vu, J. M. Wallace, and B. Bezzerides, Phys. Plasmas **1**, 3542 (1994).

79. E. A. Williams, R. L. Berger, R. P. Drake, A. M. Rubenchik, B. S. Bauer, D. D. Meyerhofer, A. C. Gaeris, and T. W. Johnston, Phys. Plasmas **2**, 129 (1995).

80. The assumption that the reference distribution function is Maxwellian is not quite correct because there is expected to be a nonvanishing heat flux at the quarter-critical surface. Future work will take this into account, where it is speculated that heat-carrying electrons propagating down the density gradient may be able to couple more efficiently with TPD-generated Langmuir waves.

81. H. X. Vu, D. F. DuBois, D. A. Russell, and J. F. Myatt, Phys. Plasmas **19**, 102708 (2012).

82. G. D. Doolen, D. F. DuBois, and H. A. Rose, Phys. Rev. Lett. **54**, 804 (1985).

83. D. A. Russell, D. F. DuBois, and H. A. Rose, Phys. Rev. Lett. **60**, 581 (1988).